Automation and Systems Issues in Air Traffic Control

Gabriela STROE*,[1], Irina-Carmen ANDREI[2]

*Corresponding author
*,[1]"POLITEHNICA" University of Bucharest, Faculty of Aerospace Engineering,
Gh. Polizu Street 1-7, Sector 1, Bucharest, 011061, Romania,
ing.stroe@yahoo.com
[2]INCAS – National Institute for Aerospace Research "Elie Carafoli",
B-dul Iuliu Maniu 220, Bucharest 061126, Romania,
andrei.irina@incas.ro, icandrei28178@gmail.com

DOI: 10.13111/2066-8201.2016.8.4.11

Received: 05 September 2016/ Accepted: 10 October 2016/ Published: December 2016

International Conference of Aerospace Sciences "AEROSPATIAL 2016"
26 - 27 October 2016, Bucharest, Romania, (held at INCAS, B-dul Iuliu Maniu 220, sector 6)
Section 7 – ATS and full Automation ATM

Abstract: *This paper is dedicated to the study and analysis of a successfully designed control system in ATM. The aircraft's motion is affected by other factors, besides the pilot controls in the form of external disturbances, such as wind, and internal errors, due to unmodelled dynamics, tracking error and system noise. Navigation equipment tracks the exact real-time location of the aircraft in 4D space and provides feedback to both the pilot in the cockpit and ATC via ADS-B. ATM was expressed as a large, decentralized, dynamic, variable size, infinite horizon, multi-parameter, constrained, nonlinear, non-causal, non-convex, multi-objective, high-dimensionality, hybrid (continuous and combinatorial), optimal control problem. Rapidly increasing growth and demand in CNS/ATM, the advanced scheme for ATM, ADS-B system which is based on digital communication is being implemented in the field of surveillance. ADS-B is a radically new technology that is redefining the paradigm of CNS in ATM today. Automatic Dependent Surveillance-Broadcast (ADS-B) is the next generation air surveillance system which supplants and complements the limitations of conventional radar, since conventional ATM radar systems will reach their limits soon due to the increases in air traffic.*

Key Words: *ATM Automation, ATC, ADS-B*

1. INTRODUCTION

Air Traffic Management ensures the safety of flight by optimizing flows and maintaining separation between aircraft. Aircraft trajectory is one of the most fundamental objects within the frame of ATM. However, partly due to the fact that aircraft positions are most of the time represented as radar plots, the time dependence is generally overlooked so that many trajectory statistics conducted in ATM are spatial only. Even in the most favorable setting, with time explicitly taken into account, the trajectory data are expressed as an ordered list of plots labeled with a time stamp, forgetting the underlying aircraft dynamics. [1-5]

Furthermore, the collection of radar plots describing the same trajectory can have tenths more samples, nearly all of them being redundant. From the trajectory design point of view,

this redundancy is a real handicap for the optimization process. In this survey, alternative trajectory representations are presented with a description of their advantages and limits. Currently those trajectories are represented by the mean of plot lists which are manipulated by ATM software. [1-5]

Every day, all aircraft trajectories are registered into large database for which a huge capacity is needed. Based on this new trajectory representation for which redundancy has been removed, the trajectories database may be strongly improved from the capacity point of view. This compressed trajectory format may also be used for improving the trajectories transmission between ATM entities. A key issue in the performance evaluation of ATM decision support tools (DST) is the distance metric that determines the similarity of trajectories. Some proposed representation may be used to enhance the trajectory distance computation. Control input includes condition and model parameters. The model refinement (and computational complexity) ranges from tabular to many degrees of freedom. [1-5]

2. OPTIMAL CONTROL FOR AIRCRAFT TRAJECTORY DESIGN

To improve the Air Traffic Management, projects have been initialized in order to compel the aircraft in position and in time (4D trajectory) so as to avoid potential conflict and allow for some optimality with respect to a given user cost index and environmental criteria (noise abatement, pollutant emission). When trajectories samples are available (from radar for instance), one can build a dedicated base which will minimize the number of coefficients for the trajectory reconstruction. [1]

Principal Component Analysis (PCA) is a mathematical procedure that uses an orthogonal transformation to convert a set of observations of possibly correlated variables into a set of values of linearly uncorrelated variables called principal components. The number of principal components is less than or equal to the number of original variables. In the physical space, a trajectory is occasionally represented as a four-dimensional flight path, following the tradition of Air Traffic Control, with time as the fourth dimension, in addition to the normally used three-dimensional representation of a path. [6-8]

The objective of the optimal control theory is to determine the control input(s) that will cause a process (i.e., the response of a dynamical system) to satisfy the physical constraints, while minimizing (or maximizing) some performance criterion. The feasibility of the trajectories is automatically ensured using this approach. [6-8]

The typical Optimal Control Problem (OCP) can be stated as follows: - Given the initial conditions, the final conditions, and an initial time, determine the final time, the control input and the corresponding state history $x(t)$ for $t \in [t_0, t_f]$ which minimize the cost function [7]

$$\mathrm{J(x,u)} = \int_{t_0}^{t_f} \mathrm{L\big(x(t),u(t)\big)dt} \tag{1}$$

Where $x(t)$ and $\mathrm{u}(t)$ satisfies differential and algebraic constraints, for all $t \in [t_0, t_f]$:

$$\begin{cases} \dot{x} - f\big(x(t),u(t)\big) = 0 \\ \quad C\big(x(t),u(t)\big) \le 0 \end{cases} \tag{2}$$

$$u_{opt} = argmin_{u \in U} H(t,x,\lambda,u) \tag{3}$$

$$H(t,x,\lambda,u) = \mathrm{L(x,u)} + \lambda^T f(x,u) \tag{4}$$

$$\dot{\lambda}\ (t) = -\frac{\partial H}{\partial x}\big(x(t), \lambda(t), u(t)\big) \tag{5}$$

During the terminal landing phase, commercial airliners are required to follow strict Air Traffic Control (ATC) rules, which guide the airplanes to follow 'virtual' three-dimensional corridors all the way to the landing strip. Furthermore, since our approach leads to very fast computation of feasible trajectories, one can use the approach over new, locally modified paths repeatedly till a satisfactory path is found. [6-8]

A major issue with almost all current trajectory optimization solvers (direct or indirect) is the fact that their computational complexity is high and their convergence strongly dependents on the initial conditions, unless certain rather stringent convexity conditions hold. As a result, the solution of trajectory optimization problem in real-time is still elusive. [7] A common line of attack for solving trajectory optimization problem in real time (or near real time) is to divide the problem into two phases: an offline phase and an online phase. The offline phase consists of solving the optimal control problem for various reference trajectories and storing these reference trajectories onboard for later online use.

These reference trajectories are used to compute the actual trajectory online via a neighboring optimal feedback control strategy typically based on the linearized dynamics. Another strategy for computing near-optimal trajectories in real-time is to use a receding horizon (RH) approach. [6-8] In a receding horizon approach a trajectory that optimizes the cost function over a period of time, called the planning horizon, is designed first. The trajectory is implemented over the shorter execution time and the optimization is performed again starting from the state that is reached at the end of the execution time. [1]

A third approach is to use a two-layer architecture, where first an acceptable path (in terms of length, safety, etc) is computed using common path-planning techniques, and then an optimal time-parameterization is imposed on this path to yield a feasible trajectory.

However, when successful, such an approach is numerically very efficient and can be implemented in real-time with current computer hardware. [6-8]

Aircraft maneuvering was one of the first areas where the optimal control theory was used to generate optimal trajectories.

The main objective is to find a time-parameterization along the path, i.e., a function $s(t)$, where $t \in [0, t_f]$), such that the corresponding time-parameterized trajectory $\big(x(s(t)),\ y(s(t)),\ z(s(t))\big)$ minimizes either the flight time t_f (emergency landing case) or fuel (terminal landing operation). [6-8]

As shown in [1-5] all control (thrust, angle of attack, load factor, etc) constraints can be mapped into constraints involving the specific kinetic energy of the aircraft, $E = \frac{v^2}{2}$ where v is the aircraft velocity of the form [6-8]

$$\underline{g}_w(s) \le E(s) \le \overline{g}_w\ (s) \tag{6}$$

$$\min_T \ \int_{s_0}^{s_f} \frac{ds}{\sqrt{2E(s)}} \tag{7}$$

$$E'(s) = \frac{T(s)}{m} - D(E(s), s) - g \cdot sin\gamma(s) \tag{8}$$

$$T_{min} \le T(s) \le T_{max} \tag{9}$$

$$\min_T \ \int_{s_0}^{s_f} T(s)ds\ ;\ \ E'(s) = \frac{T(s)}{m} - D(E(s),s) - g \cdot sin\gamma(s) \tag{10}$$

$$t'(s) = \frac{1}{\sqrt{2E(s)}};\ \underline{g}_w(s) \le E(s) \le \overline{g}_w\ (s);\ T_{min} \le T(s) \le T_{max} \tag{11}$$

$D(E(s),s)$ is the drag, T is the thrust, γ is the flight-path angle, and where prime denotes differentiation with respect to path length s.

The main advantage of these problem formulations is the reduction of the problem dimensionality that can be leveraged to solve both of these problems very efficiently and reliably. In fact, these OCPs (Optimal Control Problem) are simple enough so that the optimal switching structure of the optimal solution can be unraveled using the necessary conditions from PMP (Pontryagin's Maximum Principle). For the minimum-fuel problem the switching structure varies depending on the given TOA (Time-of-Arrival). However, for a given path and a fixed TOA, the structure is uniquely determined. This helps tremendously the convergence properties of the algorithm. [12-14]

Aircraft trajectory planning has reached enough maturity to shift the trajectory planning problem from the mathematical optimization of the aircraft trajectory to the automated parsing and understanding of desired trajectory goals, followed by their re-formulation in terms of a mathematical optimization program. [1-5]

At the operator level, the information is presented to the operator in the form of sentences expressed in natural language (e.g. that used by Air Traffic Control phraseology). At the level of trajectory planning automation, the information is presented as a mix of continuous parameters (aircraft position and speed), and discrete parameters describing mission status (completed tasks, tasks remaining to be completed). [1-5]

A natural language interpreter and task scheduler transforms the operator's requirements into tractable mathematical optimization programs that may be executed by the aircraft through its Flight Control Computer. [1-5]

The aircraft's innermost dynamics (that consist of raw aircraft dynamics and SAS-Stability Augmentation System), although critical to vehicle stability, is not shown. The main goal of using a Natural Language Interface (NLI) for interacting with a computer-based system is to minimize the workload on the operator. After the Natural Language Interface and Flight Planning and Scheduling components have converted the flight plan into a series of tasks for the aircraft to perform, the Trajectory Generation Module guides the vehicle from one task to the next, i.e. from an initial state to a desired one, through an obstacle field while optimizing a certain objective. The latter can be to minimize time, fuel or a combination of both. [6-8]

By introducing a cost function over the *T* time steps, the general trajectory optimization problem can be formulated as to [13-14]

$$\text{Minimize}_{\ \boldsymbol{X_{i,ui}}}\ \ J_T = \sum_{i=1}^{T} f_i\ \left(X_i, u_i, X_f\ \right) +\ \ f_T\left(X_T, X_f\ \right) \tag{12}$$

$$\begin{cases} X_{i+1} = AX_i + Bu_i,\ \ i = 0, \dots, T-1 \\ X_0 = X_{estim.} \\ X_i \in\ \mathcal{X}_0,\ \ i = 1, \dots, T \\ u_i \in\ \mathcal{U}_0,\ \ i = 0, \dots, T-1 \\ (x_i,\ y_i) \in\ \mathcal{D}_0,\ \ i = 1, \dots, T \\ (x_i,\ y_i) \notin\ \mathcal{O}_0,\ \ i = 1, \dots, T \end{cases} \tag{13}$$

The objective function consists of stage costs $f_i\ (X_i, u_i, X_f\ )$ corresponding to each time step- i, and a terminal cost term $f_T(X_T, X_f\ )$ that accounts for an estimate of the cost-to-go from the last state X_T in the planning horizon to the goal state X_f. [13-14]

The sets $\mathcal{X}_0$ and $\mathcal{U}_0$ represent the (possibly non-convex) constraints on the aircraft dynamics and kinematics, such as bounds on velocity, acceleration and turn rate. Here, the 0-subscript denotes the fact that these constraints can be dependent on the initial state. [15]

Lastly, the expressions $(x_i,\ y_i) \in \mathcal{D}_0$ and $(x_i,\ y_i) \notin \mathcal{O}_0$ capture the requirement that the planned trajectory points should lie inside the known region $\mathcal{D}_0$, but outside the obstacles $\mathcal{O}_0$ as given at the current time step i = 0. [16]

At the center of the CNS/ATM system there is the ADS-B system, which is based on digital communications. Traditional surveillance methods include voice reporting, visual checks, and primary and secondary surveillance radars.

However, in CNS/ATM, these methods are replaced by ADS-B, a radically new technology that is currently redefining the paradigm of communications, navigation, and surveillance in Air Traffic Management. [18]

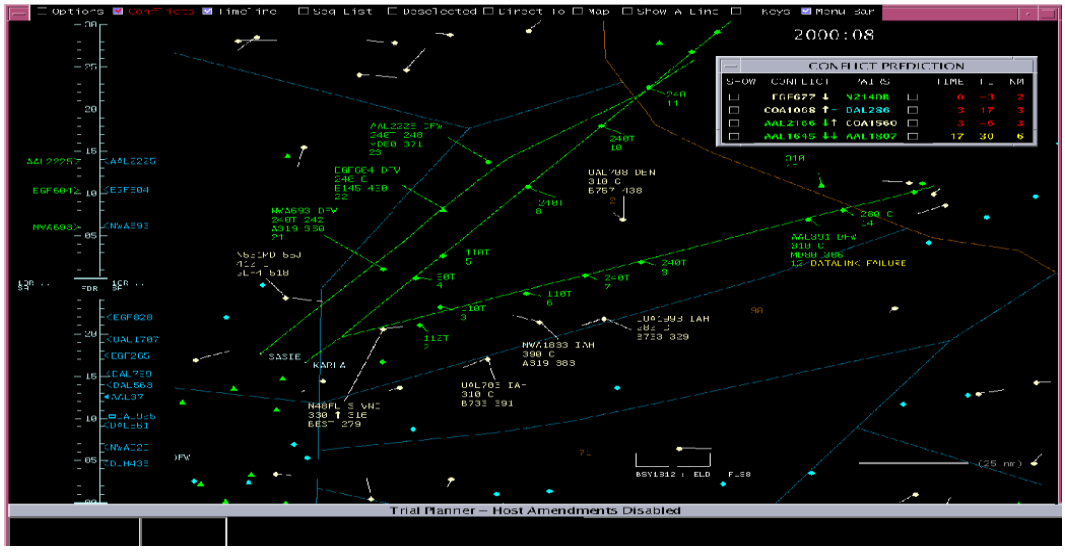

Fig. 1 Controller display for Automated Airspace Sector
[H. Erzberger, Senior Scientist NASA Ames Research Center] [18]

Already proven and certified as a viable low-cost replacement for conventional radar, ADS-B allows pilots and Air Traffic Controllers to see and control aircraft with more precision over a far larger percentage of the Earth's surface than has ever been possible before. ADS-B is a next-generation air surveillance system that will supplant and complement conventional radar, since conventional Air Traffic Management radar systems will reach their limits soon owing to the increases in air traffic.

According to recent studies, the position accuracy of conventional radar is 200 m. However, ADS-B achieves a position accuracy of 33 m. Nevertheless, although ADS-B has better position accuracy, it includes errors from the GNSS since the position information of the aircraft relies completely on the GNSS. [18]

GPS-based TCAS equipment which is capable of processing ADS-B messages may use this information to enhance the performance of TCAS, using techniques known as hybrid surveillance. [18]

3. MODELS OF TRAJECTORY CONTROL

Flying aircraft are controlled by pilots or autopilots to follow commanded trajectories. The horizontal part of the commanded trajectory can then be constructed from [12-16]

$$\dot{x_c} = V_c(t)\sin\Psi_c\ (t) + \widehat{W}_x\ (t) \tag{14}$$

$$\dot{y_c} = V_c(t)\cos\Psi_c\ (t) + \widehat{W}_y\ (t) \tag{15}$$

$\widehat{W}_x\ (t)$ and $\widehat{W}_y\ (t)$ are estimated wind components available to the aircraft.

The idea of feedback linearization is to derive the necessary control functions from a specification of desired closed-loop response dynamics. For example, the normalized lift may be used to control the aircraft altitude, and the resulting trajectory control is of second-order. The desired altitude response dynamics can be stated as [12-16]

$$\left(\ddot{h}\ - \ddot{h}_c\right) + K_{V1}\left(\dot{h} - \ \dot{h}_c\right) + \ K_{V2}\ (h - \ h_c) = 0 \tag{16}$$

where $K_{V1} > 0,\ K_{V2} > 0$ are feedback control gains. Assuming in consistence with commercial flights $\overline{T}\ \ll\ \bar{L}$, $|\gamma| \ll 1$ and for most of the times during a flight $|\phi| \ll 1$.

$$\ddot{h} = \dot{V}\ \sin\gamma + \dot{\gamma}\ \ V cos\gamma + \dot{W}_h \approx g(\bar{L} - 1) \tag{17}$$

$$\bar{L} = 1 - \frac{K_{V1}}{g}\left(\hat{\dot{h}}\ -\ \dot{h}_c\right) - \frac{K_{V2}}{g}\left(\hat{h}\ -\ h_c\right) \tag{18}$$

$$\hat{\dot{h}} = \dot{h} + n_{\dot{h}} \tag{19}$$

$$\hat{h} = h + n_h \tag{20}$$

where $n_{\dot{h}}$ and n_h are the corresponding navigation / estimation errors. [12-16]

$$K_{V1} = 2\zeta_V\omega_V \tag{21}$$

$$K_{V2} = \omega_V^2 \tag{22}$$

$$\begin{bmatrix}\xi\\ \eta\end{bmatrix} = \begin{bmatrix}\sin\Psi_c & \cos\Psi_c\\ \cos\Psi_c & -\sin\Psi_c\end{bmatrix}\begin{bmatrix}x - x_c\\ y - y_c\end{bmatrix} \tag{23}$$

$$\eta = (x - x_c)\cos\Psi_c - (y - y_c)\sin\Psi_c \tag{24}$$

$$\xi = (x - x_c)\sin\Psi_c + (y - y_c)\cos\Psi_c \tag{25}$$

$$|\Psi - \Psi_c| \ll 1\ \ ;\ \ |\gamma| \ll 1\ ;\ \ \bar{L}\ \approx 1\ ;\ \overline{T} \ll \bar{L} \tag{26}$$

$$\begin{gathered}\sin\phi \approx \frac{\mathrm{V_c}}{\mathrm{g}}\dot{\Psi}_c - \frac{K_{L1}V_c}{g}\Delta\widehat{\Psi} - \frac{K_{L2}}{g}\hat{\eta}\\ \Delta\widehat{\Psi} = \Psi - \Psi_c + n_\Psi\ \ ;\ \ \hat{\eta} = \eta + n_\eta\end{gathered} \tag{27}$$

$$\overline{T_C} = \sin\gamma + \frac{\dot{V_c}}{g} - \frac{K_{s1}}{g}\left[\hat{V} - V_c\right] \tag{28}$$

$$\overline{T_C} = \sin\gamma + \frac{\dot{V_c}}{g} - \frac{K_{s1}}{g}\left[\widehat{V_g} - V_c\right] - \frac{K_{s2}}{g}\hat{\xi} \tag{29}$$

$$\hat{V} = V + n_V\ \ ;\ \ \widehat{V_g}\ = V_g + n_V\ \ ;\ \ \hat{\xi}\ =\ \xi + n_\xi \tag{30}$$

Mathematically, the surveilled aircraft state may be expressed as [9-11]

$$x_{n,0} = x_0 + \Delta x_s \;\; ; \;\; y_{n,0} = y_0 + \Delta y_s \;\; ; \;\; h_{n,0} = h_0 + \Delta h_s \tag{31}$$

$$V_{n,0} = V_c(0) + \Delta V_s \;\; ; \;\; \Psi_{n,0} = \Psi_c(0) + \Delta\Psi_s \tag{32}$$

$$\Delta R_s = \sqrt{(\Delta x_s)^2 + (\Delta y_s)^2} \tag{33}$$

$$\dot{V_n} = \dot{V_c}(0) + \Delta\dot{V}_s \;\; ; \;\; \dot{\Psi}_n = \dot{\Psi}_c(0) + \Delta\dot{\Psi}_s \;\; ; \;\; \dot{h_n} = \dot{h_c}(0) + \Delta\dot{h}_s \tag{34}$$

$$V_n(t) = V_{n,0} + \dot{V_n}t \tag{35}$$

$$\Psi_n(t) = \Psi_{n,0} + \dot{\Psi}_n t \tag{36}$$

$$x_n(t) = x_{n,0} + W_{x,n}t + \frac{V_{n,0}}{\dot{\Psi}_n}\cos\Psi_{n,0} - \frac{\dot{V_n}}{\left(\dot{\Psi}_n\right)^2}\sin\Psi_{n,0} - \frac{V_{n,0} + \dot{V_n}t}{\dot{\Psi}_n}\cos\Psi_n(t) + \\ + \frac{\dot{V_n}}{\left(\dot{\Psi}_n\right)^2}\sin\Psi_n(t) \tag{37}$$

$$y_n(t) = y_{n,0} + W_{y,n}t + \frac{V_{n,0} + \dot{V_n}t}{\dot{\Psi}_n}\sin\Psi_n(t) - \frac{V_{n,0}}{\dot{\Psi}_n}\sin\Psi_{n,0} + \\ + \frac{\dot{V_n}}{\left(\dot{\Psi}_n\right)^2}\left[\cos\Psi_n(t) - \cos\Psi_{n,0}\right] \tag{38}$$

$$h_n(t) = h_{n,0} + \dot{h_n}t \tag{39}$$

$$W_{x,n} = \widehat{W_x} \;\; ; \;\; W_{y,n} = \widehat{W_y} \tag{40}$$

$$x_n(t) = x_{n,0} + \left(V_{n,0}\sin\Psi_{n,0} + W_{x,n}\right)t + \frac{1}{2}\left(\dot{V_n}\sin\Psi_{n,0}\right)t^2;\ \dot{\Psi}_n = 0 \tag{41}$$

$$y_n(t) = y_{n,0} + \left(V_{n,0}\cos\Psi_{n,0} + W_{y,n}\right)t + \frac{1}{2}\left(\dot{V_n}\cos\Psi_{n,0}\right)t^2\ ;\ \dot{\Psi}_n = 0 \tag{42}$$

$$a(t) = (x - x_n)\sin\Psi_n + (y - y_n)\cos\Psi_n \tag{43}$$

$$b(t) = (x - x_n)\cos\Psi_n - (y - y_n)\sin\Psi_n \tag{44}$$

$$\Delta h = h - h_n(t) = h - h_c(t) + h_c - h_n = \Delta h_c(t) + \Delta h_s + \Delta\dot{h}_s t \tag{45}$$

Where $\Delta h_c(t)$ reflects deviations of actual aircraft altitudes from commanded altitudes.

In the case of constant heading flights with small heading angle measurement errors, a simplified solution can be found. [12-16]

$$x - x_c = \xi sin\,\Psi_c + \eta cos\,\Psi_c \tag{46}$$

$$y - y_c = \xi cos\,\Psi_c - \eta sin\,\Psi_c \tag{47}$$

$$a(t) = \xi cos(\Psi_n - \Psi_c) + \eta\sin(\Psi_n - \Psi_c) + (x_c - x_n)\sin\Psi_n + (y_c - y_n)\cos\Psi_n \tag{48}$$

$$b(t) = -\xi sin(\Psi_n - \Psi_c) + \eta cos(\Psi_n - \Psi_c) + (x_c - x_n)\cos\Psi_n - (y_c - y_n)\sin\Psi_n \tag{49}$$

$$a_{max} \le \xi_{max} + \Delta R_{S,\max} + t_f \Delta V_{S,\max} \tag{50}$$

$$b_{max} \leq \eta_{max} + \Delta \mathrm{R}_{\mathrm{S,max}} + t_f \Delta \mathrm{V}_{\mathrm{n},0} \Delta \Psi_{S,max} \tag{51}$$

$$\Delta h_{max} \leq \Delta h_{c,max} + \Delta h_{s,max} \tag{52}$$

The protected zone represents a region around a given aircraft that no other aircraft should penetrate for the safety of both aircraft, and defines the minimum separation requirements.

However, in fact, inaccuracies of aircraft surveillance create uncertainties in the knowledge of aircraft state information for ground ATC and other aircraft. In order for air traffic controllers and other pilots to maintain sufficient inter-aircraft separations, they need to identify a region in which each aircraft is located over a certain time frame. [17]

On the other hand to determine practical required action ranges for the current ATC system many factors must be considered that include relative aircraft geometry, aircraft performance limits, radar sweep times, controller reaction times, communication times, and pilot response times. [17]

4. NUMERICAL SIMULATION AND CONCLUSIONS

Consider first the radar in use by Air Traffic Control. The range estimation by radar is quite accurate. But, the error in azimuth can be significant. The resulting error region would then be an ellipse with a major axis perpendicular to the line of sight to the radar. [19]

In practical implementation it is most convenient to assume a spherically shaped error region with the major axis as the diameter. For the altitude measurement Air Traffic Control uses Secondary Surveillance Radar (SSR).

Assuming a Mode C transponder, the altitude quantization error is about 100 feet. GPS receivers are now used onboard aircraft to provide accurate aircraft state measurements, and these measurements may be broadcast to the ground and other aircraft in the concept of Automatic Dependent Surveillance-Broadcast, ADS-B.

Surveillance accuracy would then depend on the onboard GPS system accuracy, and the frequency as well as effective number of digits in the broadcast.

The demonstrated dependence of the protected zone on surveillance accuracy is highly consistent with the discussions in Reynolds & Hansman [17], in which the required horizontal separation is 5 nm for controlled aircraft more than 40 nm from the radar site and 3 nm over the terminal area.

In current ATC practice, the protected zone is a standard for all aircraft and aircraft geometries with the possible exceptions of aircraft takeoffs and landings. The protected zone can most likely be reduced through improved surveillance accuracy.

If the position of an aircraft is known to a greater degree of certainty, the state-uncertainty region will be smaller. This is the same conclusion arrived at by Reynolds and Hansman [17].

The desired performance index is a probability of detection- Pd and probability of false alarm- Pfa. Since coherent detection requires phase information and, therefore is more computationally expensive, we adopt a noncoherent detection scheme. The desired range resolution determines the bandwidth of the waveform, which determines the pulse width, in the case of a rectangular waveform. Another important parameter of a pulse waveform is the Pulse Repetition Frequency (PRF). The PRF is determined by the maximum unambiguous range. The receiver's noise bandwidth is set to be the same as the bandwidth of the waveform. This is often the case in real systems.

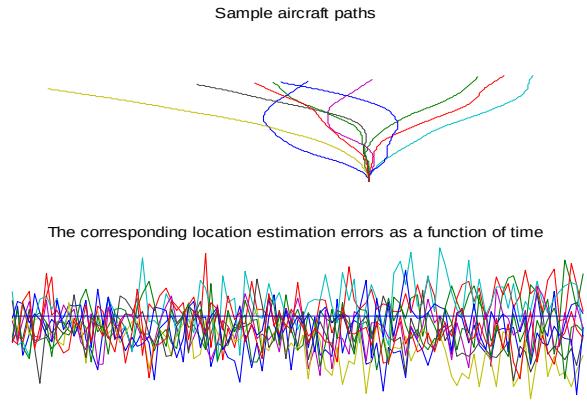

Fig. 2 Sample aircraft paths & the corresponding location estimation errors as a function of time

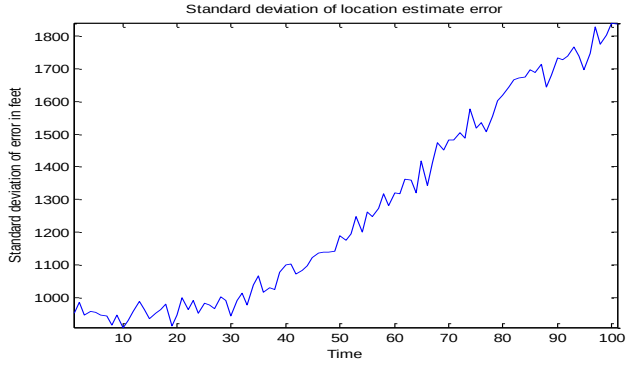

Fig. 3 Radar Tracking Simulation - Standard deviation of location estimate error

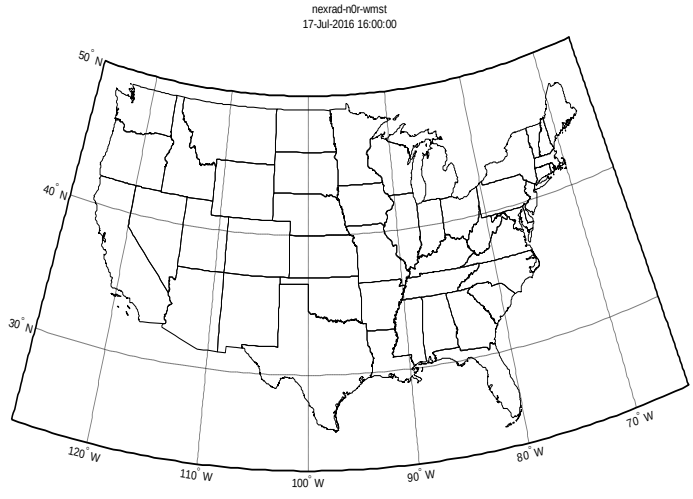

Fig. 4 Radar Tracking Simulation - 17-Jul-2016

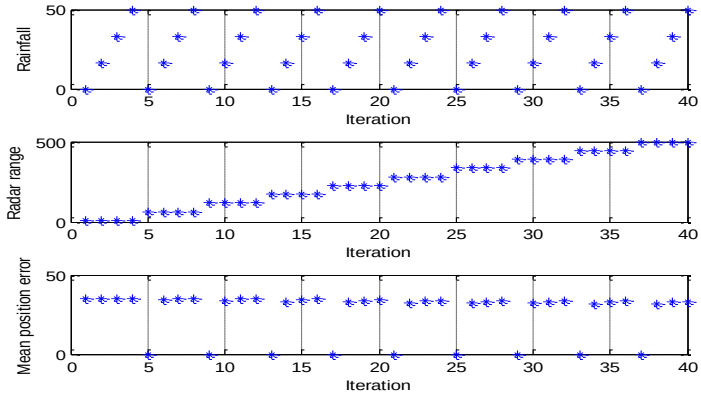

Fig. 5 Air Traffic Controller Radar Simulation Results

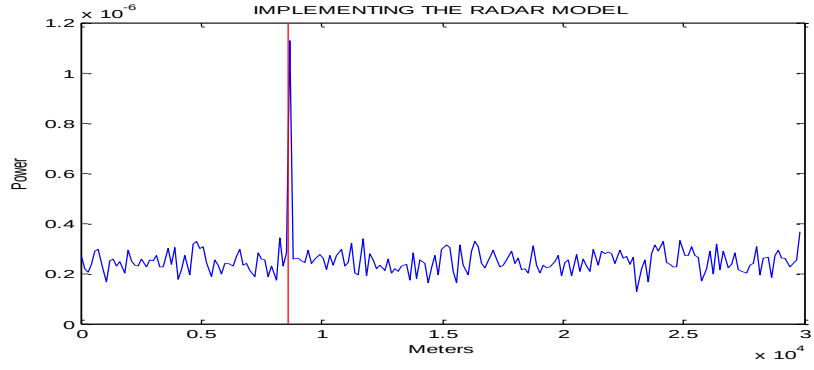

Fig. 6 Implementing the RADAR MODEL

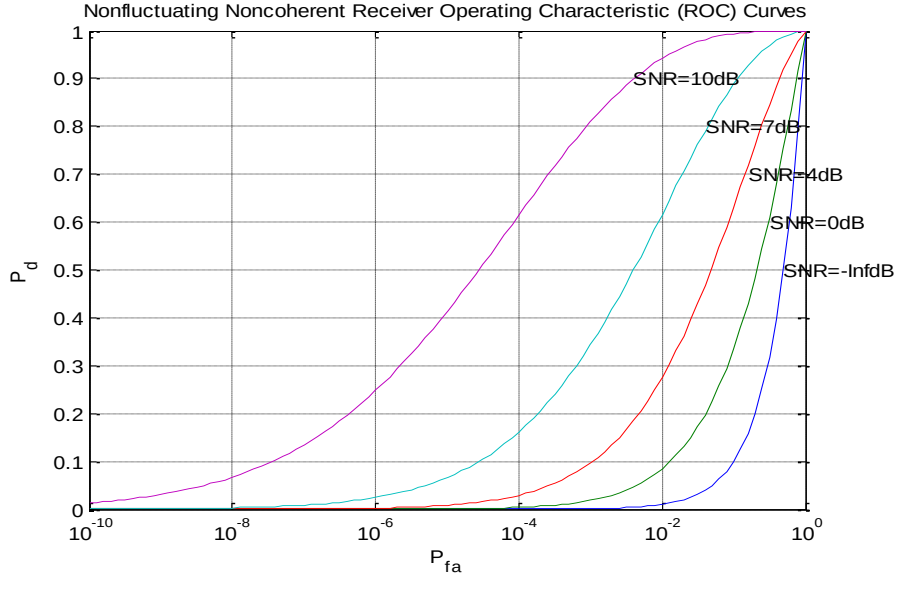

Fig. 7 Nonfluctuating Noncoherent Receiver Operating Characteristic (ROC) Curves.

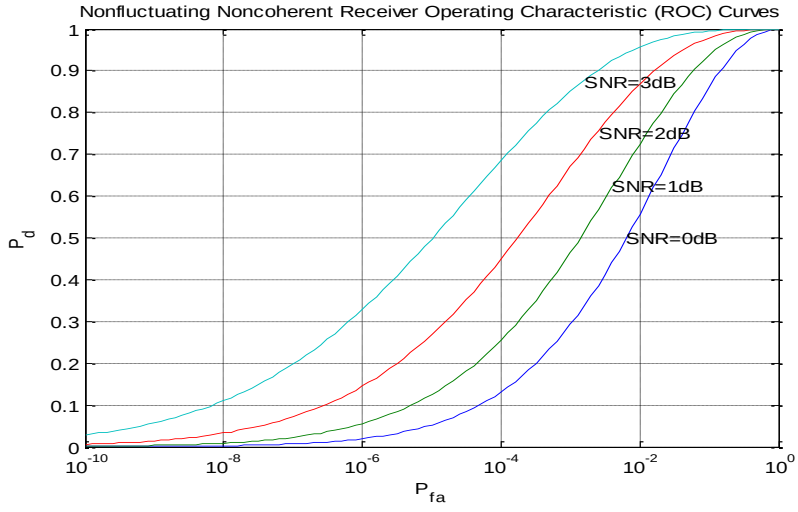

Fig. 8 Nonfluctuating Noncoherent Receiver Operating Characteristic (ROC) Curves.

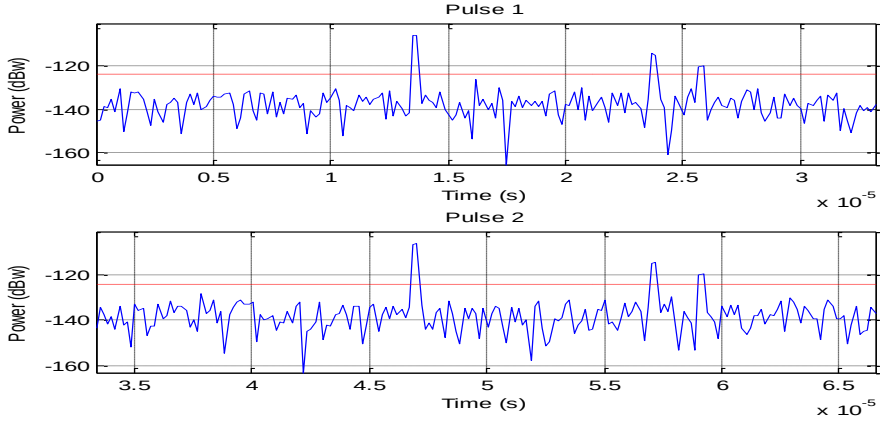

Fig. 9 Detection Threshold-the noise is white Gaussian & the detection is noncoherent

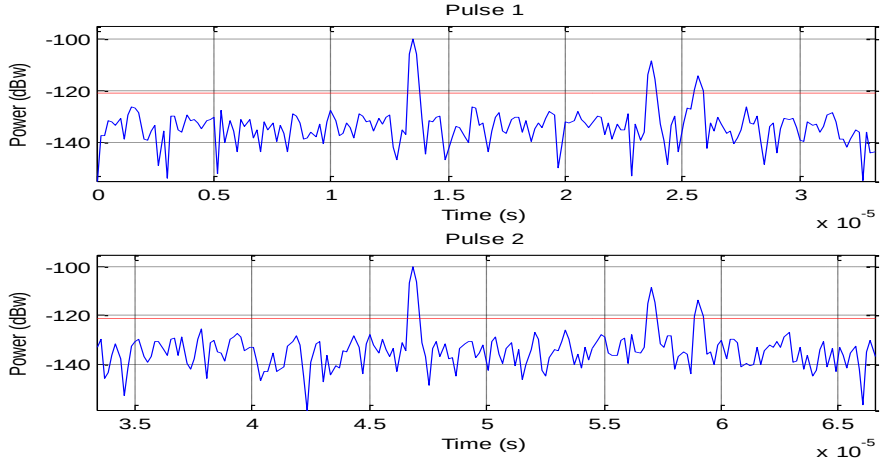

Fig. 10 The matched filter offers a processing gain which improves the Detection Threshold

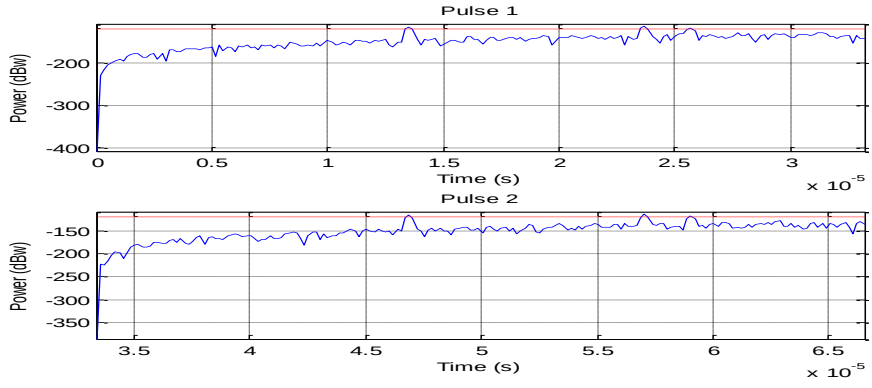

Fig. 11 Detection Threshold - after the range normalization

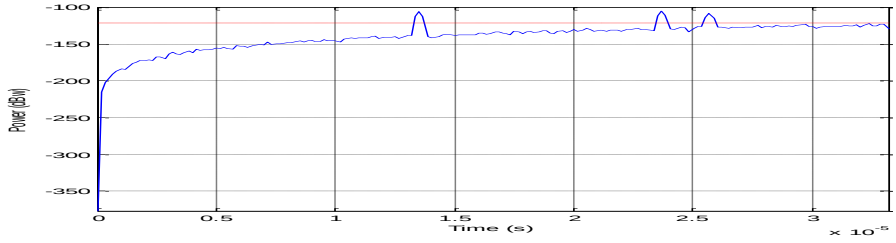

Fig. 12 The SNR by noncoherently integrating (video integration) the received pulses

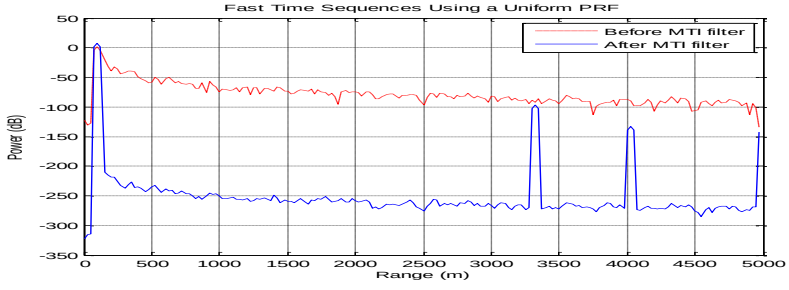

Fig. 13 Fast time sequences using a uniform PRF

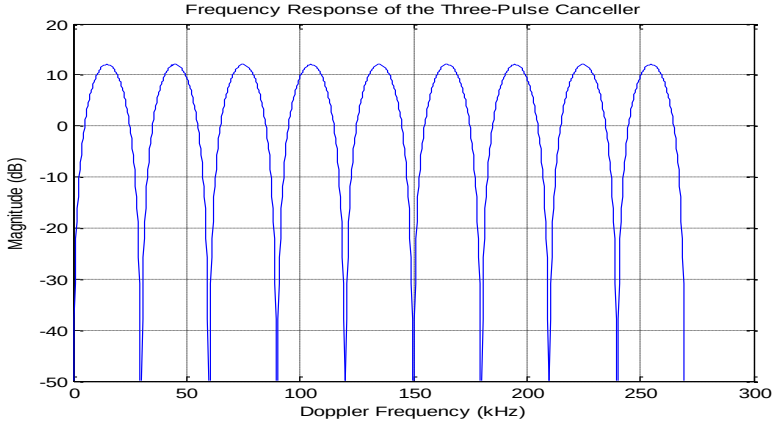

Fig. 14 Frequency response of the three - pulse canceller

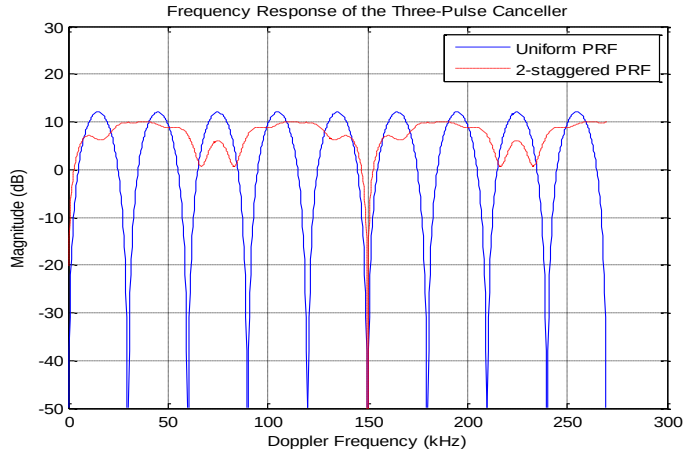

Fig. 15 Frequency response of the three-pulse canceller-blue is uniform PRF

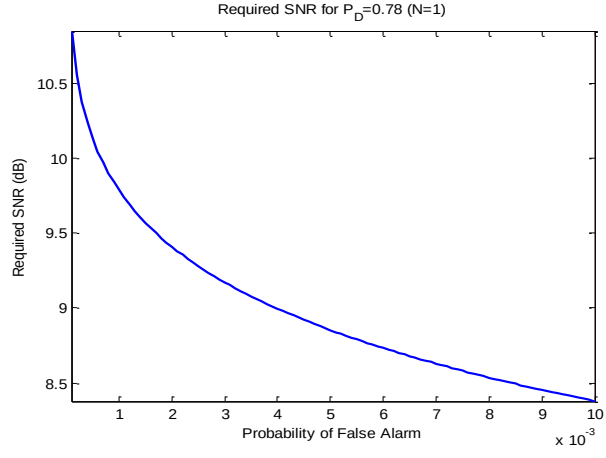

Fig. 16 Probability of False Alarm- SRN for Pd=0.78 (N=1)

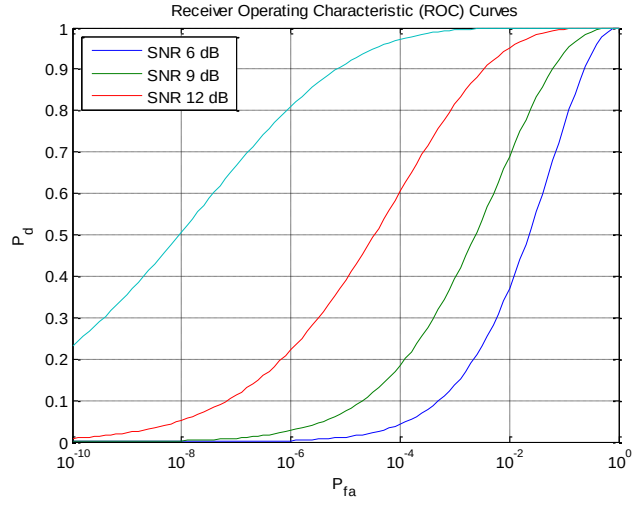

Fig. 17 Receiver Operating Characteristic (ROC) Curves

If the surveillance errors can be made small enough and become comparable to the total onboard system errors, reduction of the total onboard system errors can further reduce the protected zone. This may be achieved by using path feedback control modes and obtaining more accurate onboard measurements of wind components and aircraft states.

Furthermore, the protected zone for each aircraft and pilot can be unique. As shown, the definition of the protected zone depends upon the dynamics of the aircraft and the characteristics of the pilot. The effective dimensions of the vortex region would also depend upon the relative characteristics of the aircraft behind a given aircraft.

For example, a heavy aircraft can follow a light aircraft at a closer distance than a light aircraft can follow a heavy aircraft due to the differing capacities of roll control. Therefore, further reductions of minimum separation requirements may be achieved through individually designed and dynamically-varying protected zones. Three distinct components of the protected zone are identified as the vortex region, the safety buffer region, and the state-uncertainty region. The safety buffer region and the vortex region are essentially added to one another. These two regions must then be considered at all locations in the state-uncertainty region. A systematic procedure is presented for the analysis of the state-uncertainty region, which is defined as the contour of likely worse-case deviations of actual trajectories from nominal surveillance trajectories over a certain period of time. These deviations can be decomposed into position surveillance errors, propagation of velocity surveillance errors, and total onboard system errors consisting of flight technical errors and navigation system errors. After the surveillance errors become sufficiently small, reduction of total onboard system errors becomes important for the reduction of the protected zone.

The idea of feedback linearization is to derive necessary control functions from a specification of desired closed-loop response dynamics. For example, the normalized lift may be used to control the aircraft altitude, and the resulting trajectory control is of second-order. For estimating nominal surveillance trajectories over a long term such as for oceanic flights, the acceleration intents and the estimated wind components can vary with time. Numerical integrations can be used to obtain nominal surveillance trajectories.

The relation between Pd, Pfa and SNR can be best represented by a receiver operating characteristics (ROC) curve. To make the radar system more feasible, we can use a pulse integration technique to reduce the required SNR. Further reduction of SNR can be achieved by integrating more pulses, but the number of pulses available for integration is normally limited due to the motion of the target or the heterogeneity of the environment. For the noncoherent detection scheme, the calculation of the required SNR is, in theory, quite complex. Fortunately, there are good approximations available, such as Albersheim's equation. The synthesized signal is a data matrix with the fast time (time within each pulse) along each column and the slow time (time between pulses) along each row. The detector compares the signal power to a given threshold. In radar applications, the threshold is often chosen so that the Pfa is below a certain level. In this case, we assume the noise is white Gaussian and the detection is noncoherent. The matched filter offers a processing gain which improves the detection threshold. It convolves the received signal with a local, time-reversed, and conjugated copy of transmitted waveform. Therefore, we must specify the transmitted waveform when creating our matched filter. The received pulses are first passed through a matched filter to improve the SNR before doing pulse integration and threshold detection. The matched filter introduces an intrinsic filter delay so that the locations of the peak (the maximum SNR output sample) are no longer aligned with the true target locations. After the matched filter stage, the SNR is improved. To ensure the threshold is fair to all the targets within the detectable range, we can use a time varying gain to compensate for the

range dependent loss in the received echo. We need to perform pulse integration to ensure the power of returned echoes from the targets can surpass the threshold while leaving the noise floor below the bar. This is expected since it is the pulse integration which allows us to use the lower power pulse train. We can further improve the SNR by noncoherently integrating (video integration) the received pulses. After the video integration stage, the data is ready for the final detection stage. The detection scheme identifies the peaks and then translates their positions into the ranges of the targets. For a radar system, clutter refers to the received echoes from environmental scatters other than targets, such as land, sea or rain.

Clutter echoes can be many orders of magnitude larger than target echoes. An MTI-Moving Target Indication Radar exploits the relatively high Doppler frequencies of moving targets to suppress clutter echoes, which usually have zero or very low Doppler frequencies.

Typical MTI radar uses a high pass filter to remove energy at low Doppler frequencies. Since the frequency response of an FIR high pass filter is periodic, some energy at high Doppler frequencies is also removed. Targets at those high Doppler frequencies thus will not be detectable by the radar. This is called the blind speed problem. In many MTI systems, especially low end ones, the transmitter's power source is a magnetron. Because of this, the transmitter adds a random phase to each transmitted pulse. MTI processing uses MTI filters to remove low frequency components in slow time sequences. Because land clutter usually is not moving, removing low frequency components can effectively suppress it. Use noncoherent pulse integration to combine the slow time sequences. Exclude the first two pulses because they are in the transient period of the MTI filter. In the case before MTI filtering, both targets are buried in clutter returns. After MTI filtering, we see that most clutter returns are removed except for the direct path peak.

The noise floor is now no longer a function of range, so the noise is now receiver noise rather than clutter noise. This shows the clutter suppression capability of the three-pulse canceller. This is because the three-pulse canceller suppresses the second target because of its blind speed.

We notice recurring nulls in the frequency response. The nulls correspond to the Doppler frequencies of the blind speeds. Targets with these Doppler frequencies are cancelled by the three-pulse canceller.

One solution to the blind speed problem is to use a nonuniform PRF, or staggered PRFs. Adjacent pulses are transmitted at different pulse repetition frequencies which push the lower bound of blind speeds to a much higher value. To illustrate this, we use a two-staggered PRF- Pulse Repetition Frequency, and plot the frequency response of the three-pulse canceller.

A detector's performance is measured by its ability to achieve a certain probability of detection and probability of false alarm for a given SNR- Signal-to-Noise Ratio. Examining a detector's ROC curves provides insight into its performance. However, in real scenarios, targets can accelerate and decelerate as well as roll and pitch.

These factors cause the target's radar cross section (RCS) to vary over time. A set of statistical models called Swerling models are often used to describe the random variation in target RCS. Because the target RCS is varying, the ROC curves for fluctuating targets are not the same as the nonfluctuating ones.

In addition, because Swerling targets add random phase into the received signal, it is harder to use a coherent detector for a Swerling target. Therefore, noncoherent detection techniques are often used for Swerling targets. ROC curves are useful for analyzing detector performance, both for coherent and noncoherent systems.

REFERENCES

[1] M. Jacobson, U. T. Ringertz, Airspace constraints in aircraft emission trajectory optimization, *Journal of Aircraft* **47**, 1256–1265, 2010.
[2] W. Glover, J. Lygeros, *A stochastic hybrid model for Air Traffic Control simulation*, In Hybrid Systems: Computation and Control, Springer Berlin Heidelberg, pp. 372-386, 2004.
[3] S. Jain, P. Tsiotras, Multiresolution-based direct trajectory optimization, *Journal of Guidance, Control, and Dynamics* **31**, no. 5, 1424–1436, 2008.
[4] B. Sridhar, N. Y. Ng, H. K. Chen, Aircraft trajectory optimization and contrails avoidance in the presence of winds, *Journal of Guidance, Control, and Dynamics* **34**, 1577–1583, 2011.
[5] M. Prandini, L. Piroddi, S. Puechmorel, S. L. Brázdilová, *Toward air traffic complexity assessment in new generation Air Traffic Management Systems*, Intelligent Transportation Systems, IEEE Transactions on, 12(3), 809-818, 2011.
[6] D. Xiu, *Numerical Methods for Stochastic Computations*, Princeton University Press, Princeton, 2010.
[7] S. Boyd, L. Vandenberghe, *Convex Optimization*, Cambridge University Press, New York, 2009.
[8] M. Grant, S. Boyd, *Graph implementations for nonsmooth convex programs*, Recent Advances in Learning and Control, Edited by V. Blondel, S. Boyd, H. Kimura, pp 95–110, 2008.
[9] A. V. Rao, D. Benson, C. L. Darby, B. Mahon, C. Francolin, M. Patterson, I. Sanders, G. T. Huntington, *User's Manual for GPOPS Version 5.0: A MATLAB Software for Solving Multiple-Phase Optimal Control Problems Using hp-Adaptive Pseudospectral Methods*, University of Florida, Gainesville, 2011.
[10] M. Grant, S. Boyd, *CVX: Matlab software for disciplined convex programming, version 1.22*. URL: http://cvxr.com/cvx/, 2012.
[11] L. Moysis, M. Tsiaousis, N. Charalampidis, M. Eliadou, I. Kafetzis, *An Introduction to Control Theory Applications with MATLAB*, http://users.auth.gr/lazarosm/, 31 August 2015.
[12] M. Rauw, *FDC 1.2. - A SYMULINK Toolbox for Flight Dynamics and Control Analisys*, 2001.
[13] B. Etkin, *Dynamics of Flight-Stability and Control*, Wiley, New York, USA, 2-nd edition, 1982.
[14] D. McLean, *Automatic Flight Control System*, Prentice Hall, Hertfordshire, UK, 1990.
[15] D. McRuer, I. Ashkenas, D. Graham, *Aircraft Dynamics and Automatic Control*, Princeton University Press, July 1990.
[16] B. L. Stevens, F. L. Lewis, *Aircraft Control and Simulation*, John Wiley, USA, 1992.
[17] T. G. Reynolds and R. J. Hansman, *Analysis of Separation Minima Using A Surveillance State Vector Approach*, The 3rd USA / Europe Air Traffic Management R and D Seminar, Napoli, 2000.
[18] H. Erzberger, *The Automated Airspace Concept*, 4th USA / Europe Air Traffic Management, R&D Seminar, Santa Fe, New Mexico, USA, Dec. 3-7, 2001.
[19] * * * http://www.mathworks.com